

Peristaltic Carreau-Yasuda nanofluid flow and mixed heat transfer analysis in an asymmetric vertical and tapered wavy wall channel

Mohammad Hatami^{1,2} and D. Jing¹

¹ International Research Center for Renewable Energy, State Key Laboratory of Multiphase Flow in Power Engineering, Xi'an Jiaotong University, Xi'an, China,

² Department of Mechanical Engineering, Esfarayen University of Technology, Esfarayen, North Khorasan, Iran, e-mail: m.hatami@xjtu.edu.cn

Article Info

Article history:

Received November 5, 2020

Revised December 3, 2020

Accepted December 5, 2020

Keywords:

Carreau-Yasuda Nanofluid;
Tapered wavy channel;
Nanoparticle concentration;
Least square method;
Peristaltic flow.

ABSTRACT

In this study, two-phase asymmetric peristaltic Carreau-Yasuda nanofluid flow in a vertical and tapered wavy channel is demonstrated and the mixed heat transfer analysis is considered for it. For the modeling, two-phase method is considered to be able to study the nanoparticles concentration as a separate phase. Also it is assumed that peristaltic waves travel along X-axis at a constant speed, c . Furthermore, constant temperatures and constant nanoparticle concentrations are considered for both, left and right walls. This study aims at an analytical solution of the problem by means of least square method (LSM) using the Maple 15.0 mathematical software. Numerical outcomes will be compared. Finally, the effects of most important parameters (Weissenberg number, Prandtl number, Brownian motion parameter, thermophoresis parameter, local temperature and nanoparticle Grashof numbers) on the velocities, temperature and nanoparticles concentration functions are presented. As an important outcome, on the left side of the channel, increasing the Grashof numbers leads to a reduction in velocity profiles, while on the right side, it is the other way around.

Copyright © 2020 Regional Association for Security and crisis management and European centre for operational research.
All rights reserved.

Corresponding Author:

Mohammad Hatami,
Department of Mechanical Engineering, Esfarayen University of Technology, Esfarayen, North Khorasan, Iran.
Email: m.hatami@xjtu.edu.cn

1. Introduction

Peristaltic flow refers to a type of flow obtained due to the wavy or sinusoidal form of walls. Many applications in engineering and industrial phenomena, such as drug delivery, micro-channels, chemical plants, heat transfers, etc. include this sort of flow pattern, which Tripathi and Bég (2014) examined an application of this flow in bio-engineering through nanoparticles migration in a wavy artery. Hayat et al. (2016) used a perturbation technique to analyze a peristaltic Carreau-Yasuda nanofluid flow in a tapered asymmetric channel. Mosayebidorcheh and Hatami (Mosayebidorcheh and Hatami, 2018a, 2018b) used an efficient analytical method called least square method (LSM) for solving the peristaltic nanofluid flow between parallel and divergent walls of channels, separately.

Khan et al. (2018) considered numerically the magnetic field effect on heat transfer and fluid flow treatment of a sinusoidal wall and asymmetric channel. In another study of the MHD effect on the nanoparticles,

treatment in a U-shaped cavity was performed by Hamzah et al. (2020). They found that in their application, platelet, cylindrical, brick and spherical shapes of nanoparticles had the maximum Nusselt numbers in sequence. Also, Hatami et al. (2020) investigated the effect of rotating cylinder turbulator in a wavy channel filled by nanofluid. They reported that increasing the Reynolds number had the maximum effect on heat transfer, which observed 4.8 and 1.6 average Nusselt numbers for the cylinder wall and wavy wall, respectively. Not only these studies, but also many other studies such as Dogonchi et al. (2019), Akinshilo et al. (2017, 2020), Abdul Hakeem et al. (2020) focused on the nanofluids treatments in different areas as porous medium, between parallel and converging plates and over the plates, respectively. Ahmed et al. (2019) considered the fractional nanofluid between the vertical plates and analyzed it, mathematically, while Shukla et al. (2020) studied the entropy generation of the radiative bio-convection nanofluid under the oblique magnetic field.

Many researchers also focused on the Carreau nanofluid such as Hakeem et al. (2019), who studied the effect of exponentially variable viscosity and permeability of Carreau nanofluid flow. They categorized their results over an electromagnetic plate and in a porous medium. Furthermore, Abbasi et al. (2017) investigated the Carreau-Yasuda (C-Y) fluid in a curved channel including wavy walls and concluded that the radially varying magnetic field makes a reduction in velocity and an increment in the temperature values of the fluid. Khan et al. (2018) investigated the Carreau-Yasuda (C-Y) nanofluid chemical treatment in presence of magnetic field and found that skin friction coefficient decreased when Weissenberg number (We) is increased. Also, Tanveer et al. (2017) analyzed the peristaltic treatment of Carreau-Yasuda nanofluid in a porous medium and curved channel and concluded that greater porosity in a medium makes an improvement in fluid velocity and reduction in nanoparticle concentrations. Furthermore, Abbasi et al. (2016) investigated the viscous dissipation, Joule heating and Hall effects on the peristaltic transport of MHD Carreau-Yasuda nanofluid through an asymmetric channel.

Nanofluids, due to their wide applications in heat transfer phenomena, have motivated researchers to perform further studies and improvements. Kefayati et al. (2013) considered the water/alumina nanofluid and investigated the magnetic effect on its natural convection heat transfer. Mosayebidorcheh and Hatami (2017) also measured the natural convection heat transfer of carbon nanotube-water nanofluid between the rotating disks under thermal radiation conditions and examined the effect of important parameters on its treatments. They also modeled the two-phase (nanoparticle and base fluid) of condensation phenomena for nanofluids using the least square method (LSM) as an efficient analytical technique (Hatami, et al., 2017). Many other researchers used available analytical methods for analysis of nanofluids heat transfer due to simplicity and accuracy of these techniques. For instance, Mohyud-Din et al. (2010) used modified variational iteration method (MVIM), Mosayebidorcheh et al. (2017) used modified least square method (MLSM) for their modelling.

With numerical or analytical solution of problems available, researchers tried to optimize the outcomes by various optimization techniques. Mosayebidorcheh et al. (2015) and Hatami et al. (2016) optimized the results of heat transfer in convective-radiative longitudinal fins and circular-wavy cavity, respectively. Hatami (2017) investigated the nanoparticles migration around the heated cylinder using the Response Surface Methodology (RSM) optimization technique and found the most suitable wavy-wall shape for this application. In addition, Hatami et al. (2018) considered the Fe_3O_4 -water nanofluid heat transfer under the variable magnetic field and tried to optimize the results.

In current study, a two phase problem of heat transfer and fluid flow of peristaltic nanofluids in a two dimensional asymmetric and tapered vertical channel by LSM is solved and analyzed. The efficiency of LSM as an analytical solution of current nonlinear governing equations is examined through comparing the results by numerical outcomes. This is the first time that this kind of the nanofluid flow (Carreau-Yasuda nanofluid) is analyzed using a weighted residual method and the investigation of mixed heat transfer from this channel is considered by a parametric study on velocity, temperature and nanoparticles concentration profiles.

2. Problem description

As depicted in Fig. 1, the peristaltic and incompressible Carreau-Yasuda nanofluid flow in a two dimensional asymmetric divergent and wavy channel is considered. It is assumed that the peristaltic waves travel along the X -axis with a constant speed, c , while the Y -axis is perpendicular to it. The upper and lower surface functions of wavy walls are given by (Mosayebidorcheh and Hatami, 2018a, 2018b):

$$\begin{aligned}\bar{H}_1(\bar{X}, \bar{t}) &= -d - \bar{m}\bar{X} - b_1 \sin\left[\frac{2\pi}{\lambda}(\bar{X} - c\bar{t}) + \phi\right] \\ \bar{H}_2(\bar{X}, \bar{t}) &= d + \bar{m}\bar{X} + b_2 \sin\left(\frac{2\pi}{\lambda}(\bar{X} - c\bar{t})\right)\end{aligned}\quad (1)$$

where b_1 and b_2 are the wave amplitudes traveling along $\bar{H}_1(\bar{X}, \bar{t})$ and $\bar{H}_2(\bar{X}, \bar{t})$, respectively, ϕ represents the phase difference between the upper and lower walls and varies between $0 \leq \phi \leq \pi$, $m (\ll 1)$ is the non-uniform parameter for the tapered asymmetric channel and d shows the half-width of channel. The following relation is valid for these parameters:

$$b_1^2 + b_2^2 + 2b_1b_2d \cos \phi \leq (2d)^2 \quad (2)$$

By introducing an extra stress tensor in pseudoplastic fluid as presented in (Mosayebidorcheh and Hatami, 2018a, 2018b), the governing equations of total mass conservations, momentum and energy are given as:

$$\frac{\partial \bar{U}}{\partial \bar{X}} + \frac{\partial \bar{V}}{\partial \bar{Y}} = 0 \quad (3)$$

$$\rho_f \left(\frac{\partial}{\partial \bar{t}} + \bar{U} \frac{\partial}{\partial \bar{X}} + \bar{V} \frac{\partial}{\partial \bar{Y}} \right) \bar{U} = - \frac{\partial \bar{P}}{\partial \bar{X}} + \frac{\partial}{\partial \bar{X}} (\bar{S}_{\bar{X}\bar{X}}) + \frac{\partial}{\partial \bar{Y}} (\bar{S}_{\bar{X}\bar{Y}}) + (1 - C_0) \rho_f g \alpha (T - T_0) + (\rho_p - \rho_f) g \beta (C - C_0) \quad (4)$$

$$\rho_f \left(\frac{\partial}{\partial \bar{t}} + \bar{U} \frac{\partial}{\partial \bar{X}} + \bar{V} \frac{\partial}{\partial \bar{Y}} \right) \bar{V} = - \frac{\partial \bar{P}}{\partial \bar{Y}} + \frac{\partial}{\partial \bar{X}} (\bar{S}_{\bar{Y}\bar{X}}) + \frac{\partial}{\partial \bar{Y}} (\bar{S}_{\bar{Y}\bar{Y}}) \quad (5)$$

$$(\rho C)_f \left(\frac{\partial}{\partial \bar{t}} + \bar{U} \frac{\partial}{\partial \bar{X}} + \bar{V} \frac{\partial}{\partial \bar{Y}} \right) \bar{T} = k \left[\frac{\partial^2 \bar{T}}{\partial \bar{X}^2} + \frac{\partial^2 \bar{T}}{\partial \bar{Y}^2} \right] + (\rho c)_p D_B \left(\frac{\partial \bar{C}}{\partial \bar{X}} \frac{\partial \bar{T}}{\partial \bar{X}} + \frac{\partial \bar{C}}{\partial \bar{Y}} \frac{\partial \bar{T}}{\partial \bar{Y}} \right) + (\rho c)_p \frac{D_T}{T_m} \left(\left(\frac{\partial \bar{T}}{\partial \bar{X}} \right)^2 + \left(\frac{\partial \bar{T}}{\partial \bar{Y}} \right)^2 \right) \quad (6)$$

$$\left(\frac{\partial}{\partial \bar{t}} + \bar{U} \frac{\partial}{\partial \bar{X}} + \bar{V} \frac{\partial}{\partial \bar{Y}} \right) \bar{C} = D_B \left[\frac{\partial^2 \bar{C}}{\partial \bar{X}^2} + \frac{\partial^2 \bar{C}}{\partial \bar{Y}^2} \right] + \left(\frac{D_T}{T_m} \right) \left[\frac{\partial^2 \bar{T}}{\partial \bar{X}^2} + \frac{\partial^2 \bar{T}}{\partial \bar{Y}^2} \right] \quad (7)$$

where $\bar{S}_{\bar{X}\bar{X}}, \bar{S}_{\bar{X}\bar{Y}}, \bar{S}_{\bar{Y}\bar{X}}, \bar{S}_{\bar{Y}\bar{Y}}$ are the components of extra stress tensor, f and p represent the fluid and nanoparticles characteristics, respectively, and \bar{C} is the nanoparticles concentration, D_B is the Brownian diffusion coefficient, D_T denotes the thermophoretic diffusion coefficient. Furthermore, expression of extra stress tensor for Carreau-Yasuda fluid is (Mosayebidorcheh and Hatami, 2018a):

$$\bar{S} = \mu(\bar{\gamma}) A_1 \quad (8)$$

where the first Rivlin-Erickson tensor and apparent viscosity are, respectively:

$$A_1 = \text{grad} \bar{V} + (\text{grad} \bar{V})^T \quad (9)$$

$$\mu(\bar{\gamma}) = \mu_\infty + (\mu_0 - \mu_\infty) \left[1 + (\Gamma \bar{\gamma})^a \right]^{\frac{n-1}{a}} \quad (10)$$

With

$$\bar{\gamma} = \sqrt{2 \text{tr} (D^2)} \quad (11)$$

$$D = \frac{1}{2} \left[\text{grad} (\bar{V}) + (\text{grad} \bar{V})^T \right] \quad (12)$$

and where a and Γ are the non-dimensional and material parameters, respectively, n is the non-dimensional power law index for Carreau-Yasuda fluid. The described fluid model defines the pseudo plastic flow with asymptotic viscosities at zero and infinite shear rates. This model also predicts the results of shear thickening, shear thinning and Newtonian fluids when $n < 1$, $n > 1$ and $n = 1$, respectively. Also, for $a = 2$ the model reduces to Carreau fluid model. In this study, the Yasuda parameter is taken as $a = 1$ to study the rheological aspects of non-Newtonian fluids. The following non-dimensional parameters can be defined:

$$\begin{aligned} x = \frac{\bar{x}}{\lambda}, \quad y = \frac{\bar{y}}{d_1}, \quad t = \frac{c \bar{t}}{\lambda}, \quad u = \frac{\bar{u}}{c}, \quad v = \frac{\bar{v}}{c}, \quad \delta = \frac{d}{\lambda}, \quad h_1 = \frac{\bar{H}_1}{d}, \\ h_2 = \frac{\bar{H}_2}{d}, \quad m = \frac{\bar{m} \lambda}{d}, \quad b = \frac{b_2}{d}, \quad p = \frac{d^2 \bar{p}}{c \lambda \mu}, \quad \theta = \frac{\bar{T} - T_0}{T_1 - T_0}, \quad \text{Re} = \frac{\rho_f c d}{\mu} \\ \text{Pr} = \frac{\mu c'_f}{k}, \quad \Omega = \frac{\bar{C} - C_0}{C_1 - C_0}, \quad \text{Nb} = \frac{\tau D_B (C_1 - C_0)}{\nu}, \quad \text{Nt} = \frac{\tau D_T (T_1 - T_0)}{T_m \nu} \\ \text{Sc} = \frac{\nu}{D_B}, \quad G_t = \frac{(1 - C_0) \rho_f g \alpha d^2 (T_1 - T_0)}{c \mu}, \quad G_n = \frac{(\rho_p - \rho_f) g \beta d^2 (C_1 - C_0)}{c \mu} \end{aligned} \quad (13)$$

where δ is the wave number, Re indicates the Reynolds number, Pr is the Prandtl number, Nt the thermophoresis parameter, Nb the Brownian motion parameter, Sc denotes the Schmidt number and G_t and G_n are the local temperature and nanoparticle Grashof numbers, respectively.

By introducing certain simplifications such as low Reynolds number and excluding the pressure term by extra stress components and using stream function, the governing equations result in the following final set of equations (Mosayebidorcheh and Hatami, 2018a, 2018b):

$$\frac{\partial^2}{\partial y^2}(s_{xy}) - G_t \theta + G_n \Omega = 0 \tag{14}$$

$$\frac{\partial^2 \theta}{\partial y^2} + Nb Pr \left(\frac{\partial \Omega}{\partial y} \frac{\partial \theta}{\partial y} \right) + Nt Pr \left(\frac{\partial \theta}{\partial y} \right)^2 = 0 \tag{15}$$

$$\frac{\partial^2 \Omega}{\partial y^2} + \left(\frac{Nt}{Nb} \right) \frac{\partial^2 \theta}{\partial y^2} = 0 \tag{16}$$

where s_{xy} can be defined based on the stream function:

$$s_{xy} = \psi_{yy} \left[1 + (1 - \beta)(n - 1)We \psi_{yy} \right] \tag{17}$$

where $\beta = \frac{\mu_\infty}{\mu_0}$ is the viscosity ratio parameter and $We = \frac{\Gamma c}{d}$ the Weissenberg number.

The boundary conditions are given as:

$$\begin{cases} \psi = -\frac{F}{2}, \frac{\partial \psi}{\partial y} = 0, \theta = 0, \Omega = 0 & \text{at } y = h_1 \\ \psi = \frac{F}{2}, \frac{\partial \psi}{\partial y} = 0, \theta = 1, \Omega = 1 & \text{at } y = h_2 \end{cases} \tag{18}$$

where

$$F = \Theta + a \sin[2\pi(\bar{x} - t) + \phi] + b \sin[2\pi(\bar{x} - t)] \tag{19}$$

3. Analytical solution

As mentioned above, in this study a weighted residual method named Least Square Method (LSM) is used to resolve the Peristalsis Carreau-Yasuda nanofluid flow in the vertical and divergent channels. In this method, the residual is forced to reach zero when a trial function are applied on it as a polynomial equation of solution. In the first stage, the trial functions dependent variables are assumed so that the boundary conditions of the problem presented in Eq. (18) are satisfied:

$$\begin{aligned} \psi(y) = & -\frac{F}{2} + \frac{F}{h_2 - h_1}(y - h_1) + \frac{F}{(h_2 - h_1)^2}(y - h_1)(y - h_2) \\ & - \frac{2F}{(h_2 - h_1)^3}(y - h_1)^2(y - h_2) + c_1(y - h_1)^2(y - h_2)^2 \end{aligned} \tag{20}$$

$$\begin{aligned} \theta(y) = & \frac{1}{h_2 - h_1}(y - h_1) + c_2(y - h_1)(y - h_2) \\ & + c_3(y - h_1)^2(y - h_2) + c_4(y - h_1)^2(y - h_2)^2 \end{aligned} \tag{21}$$

$$\begin{aligned} \sigma(y) = & \frac{1}{h_2 - h_1}(y - h_1) + c_5(y - h_1)(y - h_2) \\ & + c_6(y - h_1)^2(y - h_2) + c_7(y - h_1)^2(y - h_2)^2 \end{aligned} \tag{22}$$

where c_i are the coefficients of trial functions which should be obtained using the LSM. The unknown parameters c_i are obtained by minimizing the residuals. For example, for the case of $G_t = 1, G_n = 2, Nb = 0.6, \beta = 0.1, We = 0, \theta = 1.5, \phi = \pi / 3, b_1 = 0.4, b_2 = 0.3$, the following solution is obtained:

$$\begin{aligned} \psi(y) = & 0.1363 + 0.7869y + 0.3354(y + 1.3464)(y - 1) \\ & - 0.2859(y + 1.3464)^2(y - 1) - 0.0533(y + 1.3464)^2(y - 1)^2 \end{aligned} \tag{23}$$

$$\begin{aligned} \theta(y) = & 0.5738 + 0.4262y - 0.2629(y + 1.3464)(y - 1) \\ & + 0.0599(y + 1.3464)^2(y - 1) - 0.0187(y + 1.3464)^2(y - 1)^2 \end{aligned} \tag{24}$$

$$\sigma(y) = 0.5738 + 0.4262y + 0.1807(y + 1.3464)(y - 1) - 0.0449(y + 1.3464)^2(y - 1) + 0.0202(y + 1.3464)^2(y - 1)^2 \quad (25)$$

Table 1 shows the LSM results and compares them to the numerical solution of problem for the case when $G_t = 1, G_n = 2, Nb = 0.6, \beta = 0.1, We = 0, \theta = 1.5, \phi = \pi/3, b_1 = 0.4, b_2 = 0.3$. It can be noticed that the approximate solution accuracy is acceptable, so LSM can be used for these types of problems to obtain accurate solutions.

Table 1. Comparison of the LSM results with the numerical solution of problem.

y	LSM	$u(y)$		Error	$\theta(y)$		Error
		Num			Num		
-1.346	0	0		0	0	0	0
-1.2	0.20574	0.20684		1.1E-3	0.14232	0.14423	2.0E-3
-1.0	0.47207	0.47206		1.1E-05	0.30645	0.31187	5.4E-3
-0.8	0.71208	0.70985		2.2E-3	0.44119	0.45083	9.6E-3
-0.6	0.91554	0.91146		4.1E-3	0.55203	0.56604	1.4E-2
-0.4	1.07222	1.06745		4.7E-3	0.64374	0.66155	1.8E-2
-0.2	1.171892	1.16788		4.0E-3	0.72037	0.74072	2.0E-2
0	1.20433	1.20236		1.9E-3	0.78526	0.80636	2.1E-2
0.2	1.15930	1.16015		8.5E-4	0.84101	0.86078	2.0E-2
0.4	1.02658	1.03021		3.6E-3	0.88953	0.90589	1.6E-2
0.6	0.79594	0.80123		5.3E-3	0.93201	0.94329	1.1E-2
0.8	0.45716	0.46171		4.5E-3	0.96892	0.97429	5.3E-3
1	0	0		0	1	1	0

4. Results and discussion

After solving the governing equations presented in Eq. (14)-(16) with the boundary conditions given in Eq. (18) and by using the LSM method, Table 1 presents the results and demonstrates the accuracy of LSM compared to the numerical fourth-order Runge-Kutta method. Obviously, the order of magnitude of the error for $u(y)$ is e-3 and for $\theta(y)$ it is e-2, so the LSM method can predict both velocity and temperature profiles in acceptable range, whereby its accuracy for velocity is slightly better than the accuracy for the temperature profiles. Figs. 2 and 3 demonstrate the effect of local temperature and local nanoparticle Grashof numbers (G_t and G_n) on the axial velocity profiles, respectively. From both these figures, it can be seen that the velocity profiles have different or opposite trend on the left and right sides of the channel. On the left side of the channel, increasing the Grashof numbers leads to a reduction in the velocity, while on the right side (positive Y) the opposite trend is noticed.

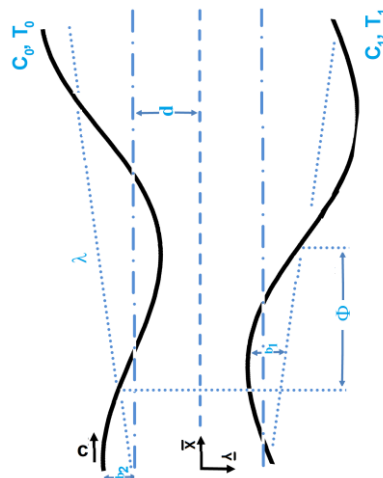


Figure 1. Schematic of the asymmetric and vertical sinusoidal channel (Mosayebidorcheh and Hatami, 2018a)

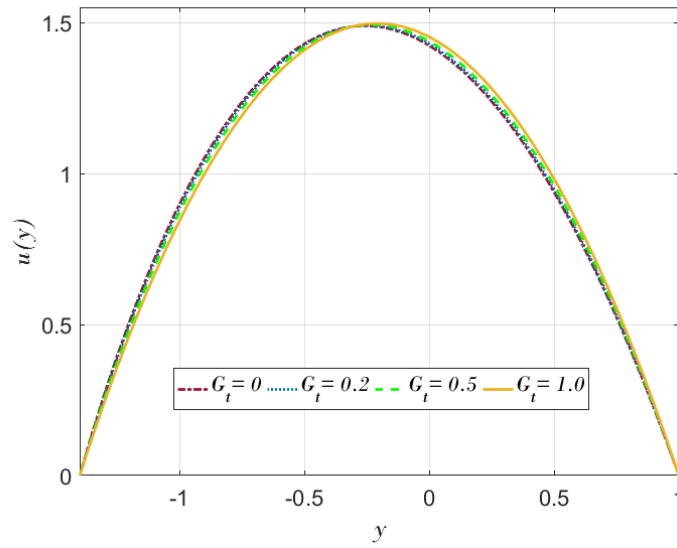


Figure 2. Axial velocity profiles for different values of G_t when $Nb = 0.3, \beta = 0.4, We = 1, \theta = 2, \phi = \pi / 3, b_1 = 0.4, b_2 = 0.3$

This trend is more pronounced for the nanoparticle Grashof number (G_n) depicted in Fig. 3.

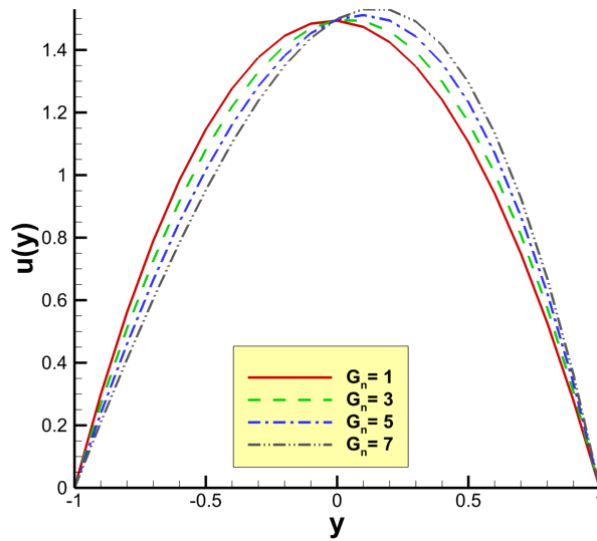


Figure 3. Axial velocity profiles for different G_n when

$$G_t = 1, G_n = 2, Nb = 0.6, \beta = 0.1, We = 0, \theta = 1.5, \phi = \pi / 3, b_1 = 0.4, b_2 = 0.3$$

Fig. 4 shows the effect of Brownian motion parameter on the temperature and nanoparticles concentration profiles, simultaneously. Increasing this parameter enhances both temperature and nanoparticles concentration due to the more intense nanoparticles movement from the walls toward the fluid.

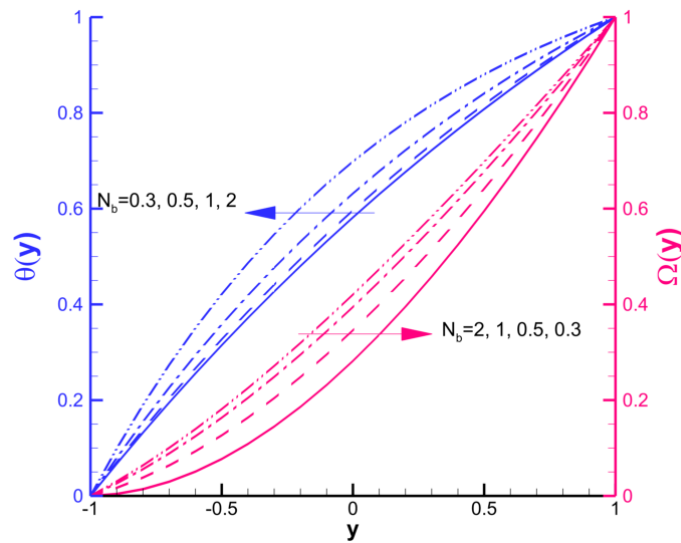


Figure 4. Temperature and nanoparticle volume fraction profiles for different N_b when $G_t = 0.5, G_n = 3, \beta = 0.4, We = 1, \theta = 2, \phi = 0, b_1 = 0.4, b_2 = 0.3$

Effects of Prandtl number on the velocity and temperature profiles for $G_t = 0.5, G_n = 3, Nb = 0.3, \beta = 0.4, We = 1, \theta = 2, \phi = 0, b_1 = 0.4, b_2 = 0.3$ are presented in Fig. 5. Increasing the Pr number has the same effect on the temperatures in the whole domain – it increases significantly the temperature values.

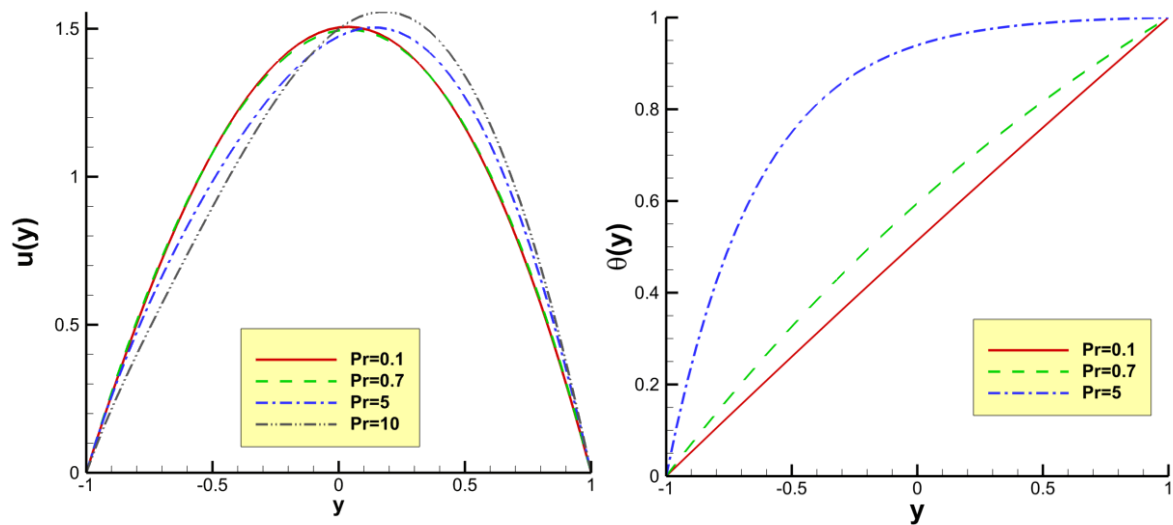


Figure 5. Axial velocity and temperature profiles for different Pr when $G_t = 0.5, G_n = 3, Nb = 0.3, \beta = 0.4, We = 1, \theta = 2, \phi = 0, b_1 = 0.4, b_2 = 0.3$

Fig. 6 demonstrates the effect of viscosity ratio parameter on the velocity values. The trend of velocity profiles, like the Grashof numbers, discussed on Figs. 2-3, is different on the left and right sides of the channel. As Hayat et al. (2018a) mentioned, for larger β the velocity profile decreases near the left wall while opposite behavior is seen towards the right wall.

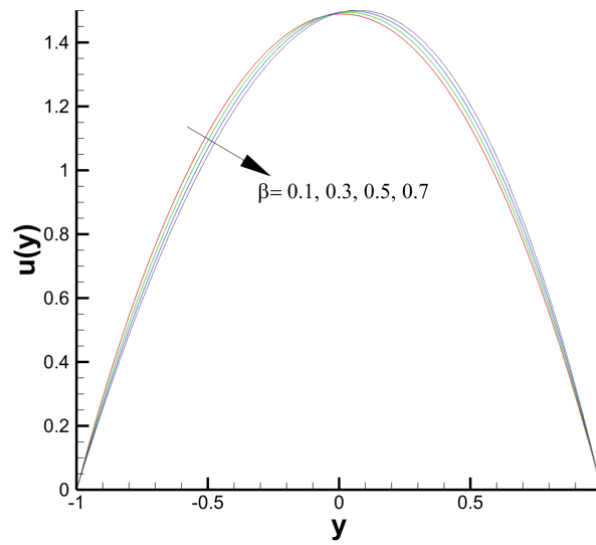


Figure 6. Axial velocity profiles for different β when $G_t = 0.5, G_n = 3, Nb = 0.3, Pr = 0.7, We = 0, \theta = 1.5, \phi = 0, b_1 = 0.4, b_2 = 0.3$

Fig. 7 reveals the impact of dimensional volume flow rate in the wave frame (Θ) onto the velocity and confirms that increasing the flow rate leads to the increase of the maximum velocity in the channel and shifts its peak to the channel center.

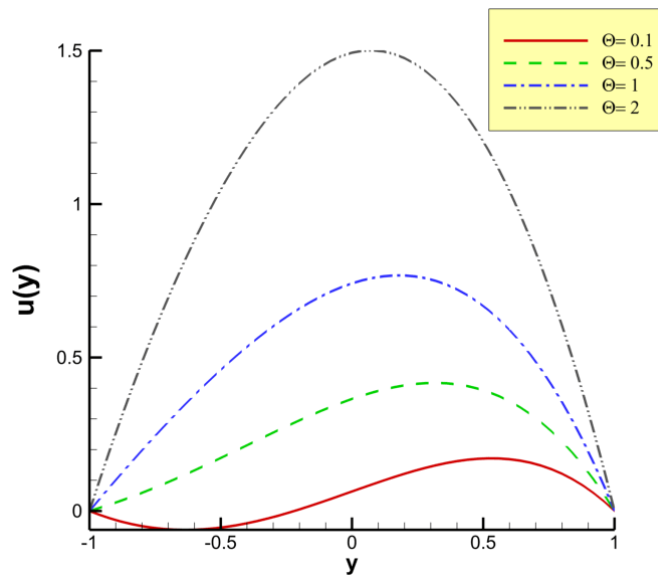


Figure 7. Axial velocity profiles for different Θ when $G_t = 0.5, G_n = 3, Nb = 0.3, Pr = 0.7, \beta = 0.7, We = 0, \phi = 0, b_1 = 0.4, b_2 = 0.3$

To show the effect of the discussed profiles (temperature, velocity and concentration) in different x sections (see Fig. 1), Fig. 8 is depicted for three x-values, namely for $x=0, x=1$ and $x=2$.

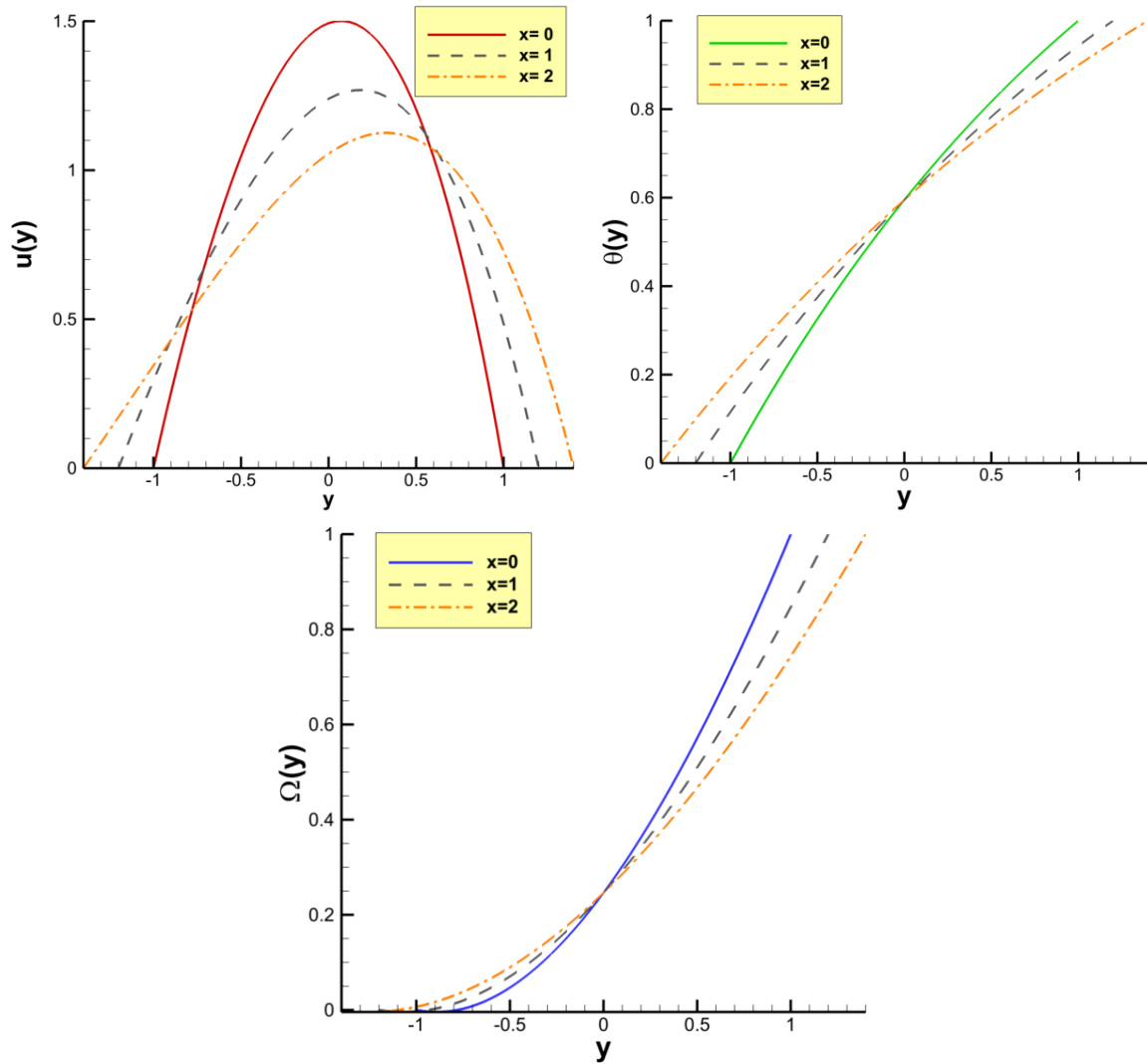
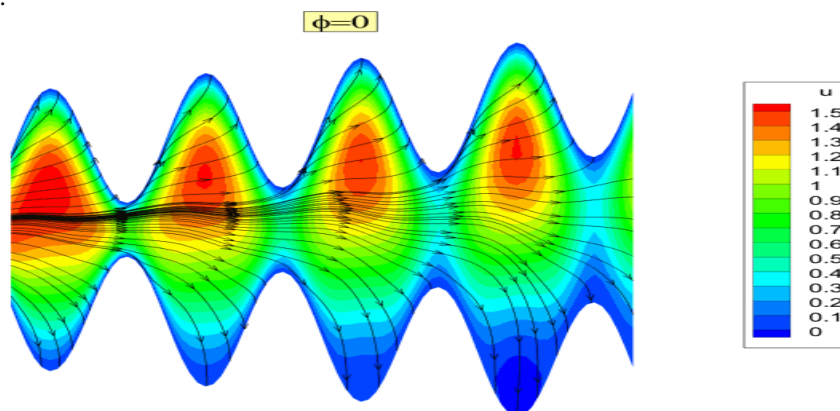


Figure 8. Axial velocity, temperature and nanoparticle volume fraction profiles for different x coordinate when $G_t = 0.5, G_n = 3, Nb = 0.3, Pr = 0.7, \beta = 0.7, We = 0, \theta = 1.5, \phi = 0, b_1 = 0.4, b_2 = 0.3$

It is clear that if the number of sections increases, it is possible to depict the contours along the x - y dimensions, as shown in Figs. 9-11 for velocity, streamlines and temperatures, respectively, and for different phase differences between the two wall sides. Fig. 9 confirms that increasing the phase difference leads to a wider cavity or vortex in the flow patterns. In addition, streamlines pattern as well as their values are more spread as seen in Fig. 10. Fig. 11 demonstrates that for lower values of φ larger temperatures occur in the channel center.



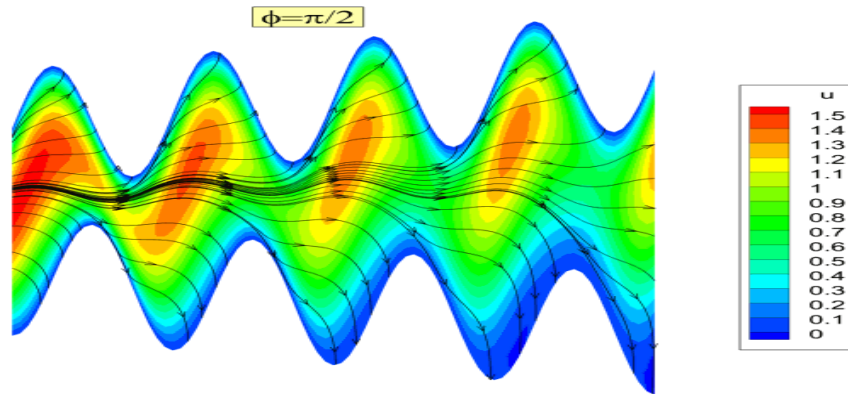


Figure 9. Velocity contour for different ϕ when $G_t = 0.5G_n = 3, Nb = 0.3, Pr = 0.7, \beta = 0.7, We = 1, \theta = 2, b_1 = 0.8, b_2 = 0.8$

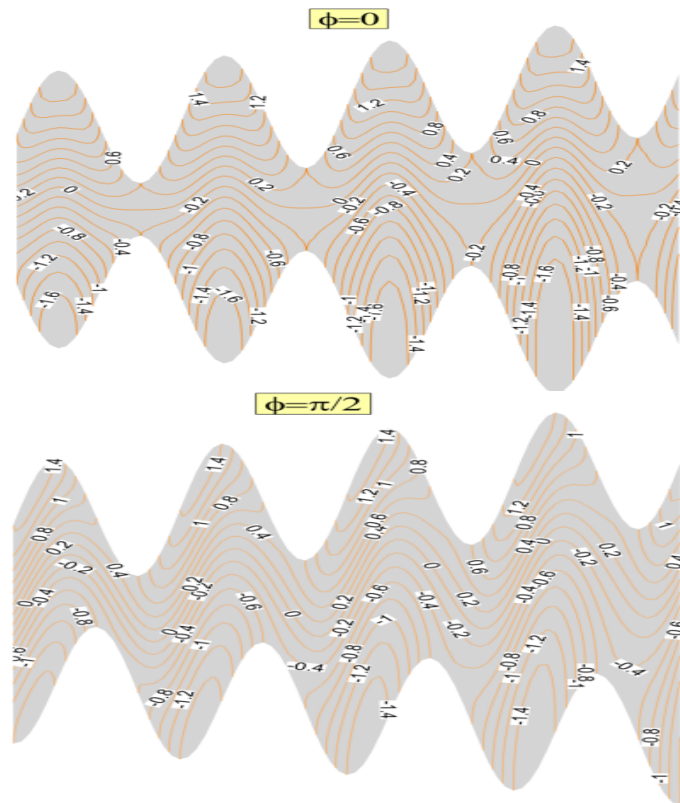


Figure 10. Streamline profiles for different ϕ when $G_t = 0.5G_n = 3, Nb = 0.3, Pr = 0.7, \beta = 0.7, We = 1, \theta = 2, b_1 = 0.8, b_2 = 0.8$

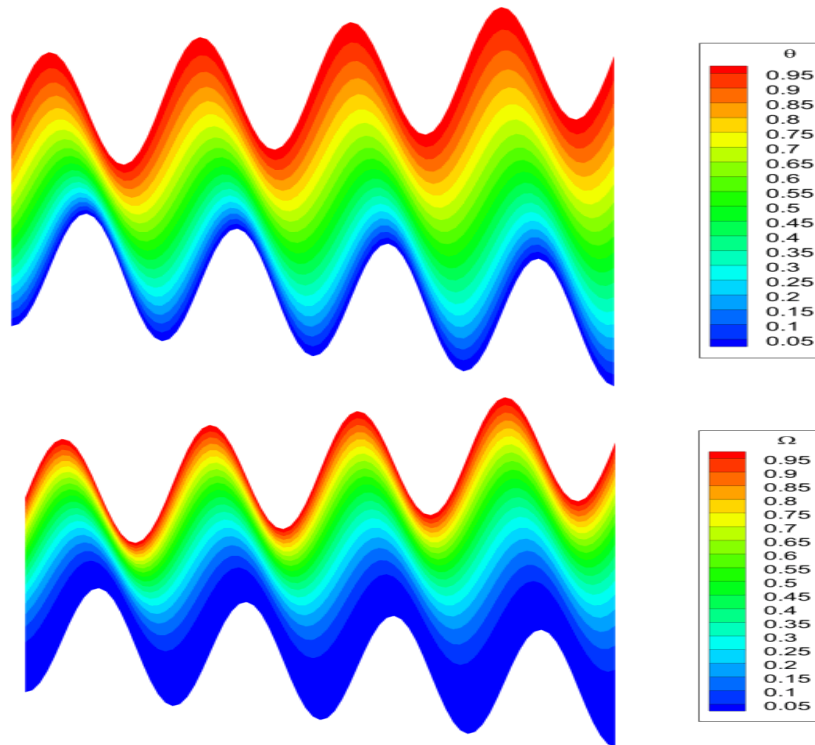


Figure 11. Temperature and nanoparticle volume fraction profiles when $G_t = 0.5, G_n = 3, Nb = 0.3, Pr = 0.7, \beta = 0.7, We = 1, \theta = 2, b_1 = 0.8, b_2 = 0.8$

5. Conclusion

In this study, solution of two phase-two dimensional modeling of asymmetric peristaltic flow and mixed heat transfer of Carreau-Yasuda nanofluids in a tapered wavy wall channel was obtained by means of the LSM analytical method. Stream function, temperature and nanoparticles concentration profiles were presented in diagrams and discussed. The outcomes are:

- On the left side of the channel, increasing the Grashof numbers leads to a reduction in velocity profiles, while on the right side, the opposite trend is seen.
- Increasing the Brownian motion parameter enhances both the temperature and the nanoparticles concentration due to the more intense nanoparticles movement from the walls toward the fluid.
- Increasing the Prandtl number has the same effect on the temperatures in the entire domain seen in enhancement of the temperature values.
- For larger viscosity ratio, the velocity profile decreases near the left wall while the opposite trend is noticed towards the right wall.
- Increasing the phase difference makes a wider vortex in the flow pattern and streamlines are more spread.

References

- Abbasi, F. M., Hayat, T. ., & Ahmad, B. (2016). Numerical analysis for peristalsis of Carreau–Yasuda nanofluid in an asymmetric channel with slip and Joule heating effects. *Journal of Engineering Thermophysics*, 25(4), 548-562.
- Abbasi, F.M., & Saba, S.A. (2017). Shehzad, Heat transfer analysis for peristaltic flow of Carreau-Yasuda fluid through a curved channel with radial magnetic field, *International Journal of Heat and Mass Transfer*, 115, 777–783.

- Abdul Hakeem, A. K., Ragupathi, P., Saranya, S., & Ganga, B. (2020). Three dimensional non-linear radiative nanofluid flow over a Riga plate." *Journal of Applied and Computational Mechanics*, 6(4), 1012-1029.
- Akinshilo, A., Adeleke Ilegbusi, T., Hafiz, M., Ali, M., & Surajo, A.-J. (2020). Heat transfer analysis of nanofluid flow with porous medium through Jeffery Hamel diverging/converging channel. *Journal of Applied and Computational Mechanics*, 6(3), 433-444.
- Akinshilo, A., Joseph, T., Olofinkua, O., & Olaye, O. (2017). Flow and heat transfer analysis of the Sodium Alginate conveying Copper Nanoparticles between two parallel plates. *Journal of applied and computational mechanics*, 3(4), 258-266.
- Anum, T., Hayat, T., Alsaedi, A., & Ahmad, B. (2017). Numerical simulation for peristalsis of Carreau-Yasuda nanofluid in curved channel with mixed convection and porous space. *PloS One*, 12(2), e0170029.
- Dogonchi, A. S., Chamkha, A. J., Seyyedi, S. M., Hashemi-Tilehnoee, M., & Ganji, D. D. (2019). Viscous dissipation impact on free convection flow of Cu-water nanofluid in a circular enclosure with porosity considering internal heat source. *Journal of Applied and Computational Mechanics*, 5(4), 717-726.
- Hakeem, A. K., Nayak, M. K., & Makinde, O. D. (2019). Effect of exponentially variable viscosity and permeability on Blasius flow of Carreau nano fluid over an electromagnetic plate through a porous medium. *Journal of Applied and Computational Mechanics*, 5(2), 390-401.
- Hamzah, K., Farooq, H., Ali, H., Hatami, M., & Jing, D. (2020). Effect of Two baffles on MHD Natural Convection in U-Shape Superposed by Solid Nanoparticle having Different Shapes. *Journal of Applied and Computational Mechanics Articles in Press*.
- Hatami, M. (2017). Nanoparticles migration around the heated cylinder during the RSM optimization of a wavy-wall enclosure. *Advanced Powder Technology*, 28(3), 890-899.
- Hatami, M., Lijun, S., Dengwei Jing, H., Günerhan, H., & Kameswaran, P.K. (2020). Rotating Cylinder Turbulator Effect on The Heat Transfer of a Nanofluid Flow in a Wavy Divergent Channel. *Journal of Applied and Computational Mechanics*.
- Hatami, M., Mosayebidorcheh, S., & Jing, D. (2017). Two-phase nanofluid condensation and heat transfer modeling using least square method (LSM) for industrial applications. *Heat and Mass Transfer*, 53(6), 2061-2072.
- Hatami, M., Song, D., & Jing, D. (2016). Optimization of a circular-wavy cavity filled by nanofluid under the natural convection heat transfer condition. *International Journal of Heat and Mass Transfer*, 98, 758-767.
- Hatami, M., Zhou, J., Geng, J., & Jing, D. (2018). Variable magnetic field (VMF) effect on the heat transfer of a half-annulus cavity filled by Fe₃O₄-water nanofluid under constant heat flux. *Journal of Magnetism and Magnetic Materials*, 451, 173-182.
- Hayat, T., Rija Iqbal, A. Tanveer, & Alsaedi, A. (2016). Mixed convective peristaltic transport of Carreau-Yasuda nanofluid in a tapered asymmetric channel. *Journal of Molecular Liquids*, 223, 1100-1113.
- Kefayati, G.H.R. (2013). Effect of a magnetic field on natural convection in an open cavity subjugated to water/alumina nanofluid using Lattice Boltzmann method. *International Communications in Heat and Mass Transfer*, 40, 67-77.
- Khan, A.A., Farooq, A., & Vafai, K. (2018). Impact of induced magnetic field on synovial fluid with peristaltic flow in an asymmetric channel, *Journal of Magnetism and Magnetic Materials*, 446, 54-67.
- Khan, M., Amna, S., Malik, M. Y., & Salahuddin, T. (2018). Chemical reaction for Carreau-Yasuda nanofluid flow past a nonlinear stretching foil considering Joule heating. *Results in Physics*, 8, 1124-1130.
- Mohyud-Din, S.T., & Yildirim, A. (2010). Solutions of tenth and ninth order boundaryvalue problems by modified variational iteration method. *Applications and Applied Mathematics*, 5(1), 11-25.
- Mosayebidorcheh, S., & Hatami, M. (2017). Heat transfer analysis in carbon nanotube-water between rotating disks under thermal radiation conditions. *Journal of Molecular Liquids*, 240, 258-267.
- Mosayebidorcheh, S., & Hatami, M. (2018a). Analytical investigation of peristaltic nanofluid flow and heat transfer in an asymmetric wavy wall channel (Part I: Straight channel). *International Journal of Heat and Mass Transfer*, 128, 790-799.

- Mosayebidorcheh, S., & Hatami, M. (2018b). Analytical investigation of peristaltic nanofluid flow and heat transfer in an asymmetric wavy wall channel (Part II: Divergent channel). *International Journal of Heat and Mass Transfer*, 126, 800-808.
- Mosayebidorcheh, S., Hatami, M., Mosayebidorcheh, T., & Ganji, D.D. (2015). Optimization analysis of convective–radiative longitudinal fins with temperature-dependent properties and different section shapes and materials, *Energy Conversion and Management*, 106, 1286–1294.
- Mosayebidorcheh, S., Tahavori, M.A., Mosayebidorcheh, T., & Ganji, D.D. (2017). Analysis of nano-bioconvection flow containing both nanoparticles and gyrotactic microorganisms in a horizontal channel using modified least square method (MLSM), *Journal of Molecular Liquids*, 227, 356–365.
- Najma, A., Shah, N.A., Ahmad, B., Shah, S.I., Ulhaq, S., & Rahimi Gorji, M. (2019). Transient MHD convective flow of fractional nanofluid between vertical plates. *Journal of Applied and Computational Mechanics*, 5(4), 592-602.
- Nisha, S., Rana, P., Kuharat, S., & Beg, O.A. (2020). Non-similar radiative bioconvection nanofluid flow under oblique magnetic field with entropy generation. *Journal of Applied and Computational Mechanics*.
- Tripathi, D., & O. Anwar Bég. (2014). A study on peristaltic flow of nanofluids: Application in drug delivery systems. *International Journal of Heat and Mass Transfer*, 70, 61-70.